Modelling of Non-Linear Aerodynamics During Limit Cycle Oscillations

A. Sedaghat, G. A. Vio, J. E. Cooper, and J. R. Wright
Manchester School of Engineering, Manchester University, Oxford Road, Manchester, M13 9PL, UK

Abstract
This paper describes a preliminary investigation into the use of unsteady CFD results for modelling the non-linear aerodynamic forces acting on lifting surfaces. Unsteady Euler calculations were carried out at transonic speeds using a simple two-degrees-of-freedom aeroelastic wing model. The lift and moment coefficients resulting from prescribed heave and pitch inputs were determined for a range of Mach numbers. A non-linear model was then identified. A good agreement between the responses of this model and the results from the CFD model were obtained.

1. Introduction

It is usual for aeroelastic calculations and flutter clearance to be made assuming linear aerodynamics and a linear aircraft structure. However, the influence of non-linearities on modern aircraft is becoming increasingly important [1] and the requirement for more accurate predictive tools grows stronger. These non-linearities can be due to structural (free-play, backlash, cubic stiffness), aerodynamic (moving shocks and transonic effects) or control (time delays, control laws) phenomena.

Vibration behaviour such as Limit Cycle Oscillations (LCO) can only occur in non-linear systems [2,3]. Consequently, it is not possible to predict LCO using a purely linear analysis and such an analysis is becoming less accurate as aircraft structures are designed to be more efficient. The study of LCO has become increasingly important over the last few years, although such problems have been noted since the 1970s.

There is an urgent need is for a predictive capability of non-linear aeroelastic phenomena. Such a ability would enable flight flutter tests to be completed faster and with a greater degree of safety. It is of particular interest to determine:

- whether an aircraft will experience Limit Cycle Oscillations and/or Flutter
- whereabouts in the flight envelope LCO phenomena will occur
- the precise nature of the LCO.

Although not desirable, LCO is essentially a fatigue problem, whereas flutter is usually catastrophic and must be avoided at all costs. An accurate LCO/flutter prediction capability would reduce significantly the amount of flights required in any flight clearance test programme with current costs being estimated at around $70k per test flight.

There has been much work in recent years [2-4] devoted towards the characterisation of non-linear aeroelastic behaviour, including LCO. This work has primarily consisted of simulating the response of the aeroelastic system through numerical integration, although there are a few known instances of experimental verification [5]. Nearly all of the effort has been devoted towards the effects of structural non-linearities, though some attention has been made towards investigating the effect of non-linearities in aeroservoelastic systems [6].

Much effort has been devoted [7,8] to improving the unsteady modelling capability through the coupling of the aerodynamic and structural grids. Significant headway has been made towards solving the problem, particularly in the transonic region. However, there are still major problems inherent due to the enormous computational resources required, even for the simplest cases.

This paper is part of a research effort investigating the use of Normal Form theory [9] to predict the behaviour of non-linear aeroelastic systems. The idea of the approach is to do away with the need for extensive computational simulations at every point in the flight envelope. However, the methodology is not seen as replacement for extensive CFD

modelling, but as a guide to determine the critical parts of the flight envelope that should be investigated using the sophisticated CFD methods.

2. Governing Aeroelastic Equations

Consider the two-degrees-of-freedom aerofoil shown in Figure 1 that can oscillate in heave and pitch. The heave deflection is denoted by h, positive in the downward direction, α is the pitch angle about the elastic axis, positive with the nose up. The elastic axis is located at a distance a_hb from the mid-chord while the mass centre is located at a distance x_αb from the elastic axis. Both distances are positive when measured towards the trailing edge of the aerofoil. The integro-differential aeroelastic equations of motion are used here in non-dimensional form. For incompressible fluids at speed U, they are written in the usual form [10] as

$$\xi'' + x_\alpha \alpha'' + 2\zeta_\xi \frac{\overline{\omega}}{U}\xi' + \left(\frac{\overline{\omega}}{\overline{U}}\right)^2 \xi = -\frac{1}{\pi\mu} C_L(\tau) + \frac{P(\tau)}{mU^2}$$

$$\frac{x_\alpha}{r_\alpha^2}\xi'' + \alpha'' + 2\zeta_\alpha \frac{1}{U}\alpha' + \left(\frac{1}{\overline{U}}\right)^2 \alpha = \frac{2}{\pi\mu r_\alpha^2} C_M(\tau) + \frac{Q(\tau)}{mU^2 r_\alpha^2} \tag{1}$$

where ξ=h/b is the non-dimensional displacement. The expressions for $C_L(\tau)$ and $C_M(\tau)$ are

$$C_L(\tau) = \pi\left(\xi'' - a_h\alpha'' + \alpha'\right) + 2\pi\phi(\tau)\left\{\alpha(0) + \xi'(0) + \left(\frac{1}{2} - a_h\right)\alpha'(0)\right\}$$
$$+ 2\pi\int_0^\tau \phi(\tau-\sigma)\left(\alpha'(\sigma) + \xi''(\sigma) + \left(\frac{1}{2} - a_h\right)\alpha''(\sigma)\right)d\sigma$$

$$C_M(\tau) = \frac{\pi}{2}a_h\left(\xi'' - a_h\alpha''\right) - \frac{\pi}{2}\left(\frac{1}{2} - a_h\right)\alpha' - \frac{\pi}{16}\alpha''$$
$$+ \pi\left(\frac{1}{2} + a_h\right)\phi(\tau)\left\{\alpha(0) + \xi'(0) + \left(\frac{1}{2} - a_h\right)\alpha'(0)\right\}$$
$$+ \pi\left(\frac{1}{2} + a_h\right)\int_0^\tau \phi(\tau-\sigma)\left(\alpha'(\sigma) + \xi''(\sigma) + \left(\frac{1}{2} - a_h\right)\alpha''(\sigma)\right)d\sigma \tag{2}$$

where the Wagner function $\phi(\tau)$ is given by

$$\phi(\tau) = 1 - \psi_1 e^{-\varepsilon_1\tau} - \psi_2 e^{-\varepsilon_2\tau} \tag{3}$$

and $P(\tau)$ and $Q(\tau)$ are the externally applied forces and moments, respectively.

Having applied the Wagner function, the integro-differential equation (1) can be rewritten in a general form containing only differential operators using the following transformation

$$w_1 = \int_0^\tau e^{-\varepsilon_1(\tau-\sigma)}\alpha(\sigma)d\sigma$$
$$w_2 = \int_0^\tau e^{-\varepsilon_2(\tau-\sigma)}\alpha(\sigma)d\sigma$$
$$w_3 = \int_0^\tau e^{-\varepsilon_1(\tau-\sigma)}\xi(\sigma)d\sigma \tag{4}$$
$$w_4 = \int_0^\tau e^{-\varepsilon_2(\tau-\sigma)}\xi(\sigma)d\sigma$$

from which the system (1) can be rewritten [11] as

$$c_0\xi'' + c_1\alpha'' + c_2\xi' + c_3\alpha' + c_4\xi + c_5\alpha + c_6 w_1 + c_7 w_2 + c_8 w_3 + c_9 w_4 + \left(\frac{\overline{\omega}}{\overline{U}}\right)^2\xi = f(\tau)$$

$$d_0\xi'' + d_1\alpha'' + d_2\alpha' + d_3\alpha + d_4\xi' + d_5\xi + d_6 w_1 + d_7 w_2 + d_8 w_3 + d_9 w_4 + \left(\frac{1}{\overline{U}}\right)^2\alpha = g(\tau) \tag{5}$$

The coefficients c_0, c_1, …,c_9,d_1,…, $d9$ are given in the appendix A of [11]. $f(\tau)$ and $g(\tau)$ are functions depending on the initial conditions and external forces, and are given by

$$f(\tau) = \frac{2}{\mu}\left(\left(\frac{1}{2} - a_h\right)\alpha(0) + \xi(0)\right)\begin{pmatrix}\psi_1\varepsilon_1 e^{-\varepsilon_1\tau} + \\ \psi_2\varepsilon_2 e^{-\varepsilon_2\tau}\end{pmatrix} + \frac{P(\tau)b}{mU^2}$$

$$g(\tau) = -\frac{\left(1 + 2a_h\right)}{2r_\alpha^2} f(\tau) + \frac{Q(\tau)}{mU^2 r_\alpha^2} \tag{6}$$

By introducing a variable vector $X = (x_1, x_2, \ldots, x_8)^T$ defined as

$$x_1 = \alpha, \quad x_2 = \alpha', \quad x_3 = \xi, \quad x_4 = \xi'$$
$$x_5 = w_1, \quad x_6 = w_2, \quad x_7 = w_3, \quad x_8 = w_4 \tag{7}$$

the coupled equations given in (5) can now be written as a set of eight first order ordinary differential equations $X' = f(X, \tau)$ such that

$$\begin{cases} x_1' = x_2 \\ x_2' = \left(c_0 H - d_0 P\right) / \left(d_0 c_1 - c_0 d_1\right) \\ x_3' = x_4 \\ x_4' = \left(-c_1 H + d_1 P\right) / \left(d_0 c_1 - c_0 d_1\right) \\ x_5' = x_1 - \varepsilon_1 x_5 \\ x_6' = x_1 - \varepsilon_2 x_6 \\ x_7' = x_3 - \varepsilon_1 x_7 \\ x_8' = x_3 - \varepsilon_2 x_8 \end{cases} \tag{8}$$

where

$$\begin{aligned} P &= c_2 x_4 + c_3 x_2 + c_4 x_3 + c_5 x_1 + c_6 x_5 + c_7 x_6 + \\ &\quad c_8 x_7 + c_9 x_8 - f(\tau) \\ H &= d_2 x_2 + d_3 x_1 + d_4 x_4 + d_5 x_3 + d_6 x_5 + d_7 x_6 + \\ &\quad d_8 x_7 + d_9 x_8 - g(\tau) \end{aligned} \tag{9}$$

Equation (8) can be integrated numerically using the Runge-Kutta method once the initial conditions $\alpha(0), \alpha'(0), \xi(0), \xi'(0)$ are given.

3. Unsteady CFD Model

An unsteady transonic CFD code [12] developed at the University of Glasgow has been used in this work. Two types of motion were used to produce data for this identification. These motions are specified as

1) Free response to a step input in pitch and plunge,
2) Prescribed sinusoidal motion in pitch and plunge,

The free response case was used to determine whether the motion at a particular condition was damped or whether flutter or LCOs resulted. The prescribed motion was then applied at particular flight conditions to investigate the relationship between the lift and moment coefficents and the heave and pitch motions. It is hoped to be able to curve-fit the aerodynamics and to introduce these terms into the non-linear prediction process.

4. Results and Discussion

For the wing model shown in the figure 1, the following geometrical values are used

$$\begin{aligned} &a_h = -0.2, \quad \mu = 10, \quad x_\alpha = 0.2, \quad \bar{U} = 1.9 \\ &\zeta_\xi = \zeta_\alpha = 0, \quad r_\alpha = 0.54, \quad \bar{\omega} = 0.34. \end{aligned} \tag{10}$$

The CFD computations were carried out over a range of Mach numbers and speeds using the step response mode to determine the type of response. From figure 2, it is observed that at Mach number 0.8, the aeroelastic system exhibit a simple classical LCO. However for the slightly higher Mach number of 0.85, the interesting feature of a non-linear divergence combined with a LCO is observed. For the higher Mach number of 1.07, the oscillation damped away as the transonic non-linear effect is diminished.

For three cases, Mach numbers of 0.8, 0.85, and 1.07, the wing model was excited with a prescribed sinusoidal motion in the pitch mode using the determined LCO frequency obtained from the step response solutions. The computed lift and moment coefficients and the frequency contents of the moment coefficient are shown in the figures 3-5, for Mach numbers 0.8, 0.85, and 1.07 respectively. At the lowest speed, the classical LCO frequency content of the lift coefficient contains a dominant frequency along with significant 3rd and 5th harmonics. There is a much greater frequency content at Mach number 0.85, suggesting a stronger non-linear flow-structure interaction at this particular flow condition. For the higher Mach number of 1.07, the first mode is only observed in the frequency content of the moment coefficient implying that the aerodynamic forces are linear. The corresponding plots for the heave motion all resulting in a single frequency linear relationship.

Figure 6 shows the restoring force plot for the moment coefficient and the corresponding error plot for different order of polynomial fits. Thus, a cubic non-linear function can adequately represent the non-linear behaviour of the aerodynamic forces for transonic inviscid flows.

Restoring force plots for C_L and C_M for a presribed sinusoidal amplitude of 6°at the different Mach numbers are plotted in the figure 7-9. A strong non-linear behaviour can be observed for M = 0.85.

At the prescribed non-dimensional speed ($\overline{U}$) and Mach number of $M_\infty = 0.85$, the amplitude of approximately 12 degrees in pitch and the frequency of 0.1 (rad/sec) are obtained using impulse response CFD computation.

A simple cubic term was added to the aerodynamic model terms such that

$$C_{L\,N} = C_L + \pi\mu\,\beta_\xi \left(\frac{\overline{\omega}}{\overline{U}}\right)^2 \xi^3$$
$$C_{M\,N} = C_M - \frac{\pi\mu\, r_\alpha^2}{2}\beta_\alpha \left(\frac{1}{\overline{U}}\right)^2 \alpha^3 \qquad (12)$$

moment curve slopes. The coefficient β_ξ and β_α were tuned to fit the data. A curvefitting process is currently under development

The LCO behaviour obtained using Runge-Kutta numerical time integration of the aeroelastic model (8) with non-linear aerodynamics (12) was compared with CFD results in the Figure 10. It can be seen that even for such a simplistic model there is a reasonable agreement.

6. Conclusions

The response to a step input of a transonic coupled CFD / structure model at various conditions was examined in order to determine when LCO occurred. Prescribed sinusoidal motions were then input at the critical frequencies to investigate the behaviour of the lift and moment coefficents when LCO occur. It was found that there was evidence of non-linearities in the moment coefficient when a pitching motion was applied for the classical LCO, and the amount of non-linearity increased for the non-linear divergence LCO motion. A simple cubic non-linear aerodynamic term was included into the mathematical model and it was found that this produced similar classical LCO motions compared to the CFD code. Further work is continuing to develop a general NARMAX type model of the non-linear aerodynamic forces and moments.

7. References

1. AGARD CP566 *Advanced Aeroservoelastic Testing and Data Analysis* (1995).
2. S.J. Price, H. Alighanbari & B.H.K. Lee, *The Aeroelastic Response of a 2 Dimensional Aerofoil with Bilinear and Cubic Structural Non-Linearities* J.Fluid and Structures v9 pp 175-193 (1995).
3. G. Dimitriadis & J.E. Cooper, *Limit Cycle Oscillation Control and Suppression* Aero Journal v103 pp 257-263 (1999).
4. Z.C. Yang & L.C. Zhao, *Analysis of Limit Cycle Flutter of an Airfoil in Incompressible F*low J. Sound and Vibration v123 n1 pp 1 – 13 (1988)
5. M.Holden, R Brazier & A. Cal, *Effects of Structural Non- Linearities on a Tailplane Flutter Mode* Int. Forum on Aeroelasticity and Structural Dynamics paper 60 (1995).
6. J.E. Cooper & G. Dimitriadis *Characterisation of Non-Linear Aeroservoelastic Behaviour* RTO Specialists' Meeting on Structural Aspects of Flexible Aircraft Control Paper 8 (1999)
7. AGARD CP 507 *Transonic Unsteady Aerodynamics and Aeroelasticity* (1992).
8. AGARD Report 822. *Numerical Unsteady Aerodynamics and Aeroelastic Simulation* (1998).
9. A.Y.T. Leung, Q.C. Zhang & Y.S. Chen, *Normal Form Analysis of Hopf Bifurcation Exemplified by Duffing's Equation* Journal of Shock and Vibration v1 pp 233-240 (1994).
10. Y.C. Fung, *An Introduction to the Theory of Aeroelasticity*, Wiley, New York, (1995).
11. A. Sedaghat, J.E. Cooper, J. R. Wright & A.Y.T. Leung, *Prediction of Non-linear Aeroelastic Instabilities*, ICAS. (2000).
12. K.J. Badcock G. Sim & B.E. Richards, *Aeroelastic studies using transonic flow CFD modelling* Int. Forum on Aeroelasticity and Structural Dynamics Paper 18 (1995)
13. S. Chen & S.A. Billings, *Representations of Non-Linear Systems: the NARMAX Model* Int.J.Control v49 n3 pp 1013 – 1032 (1989).
14. R. L. Bisplinghoff, H. Ashley and R. L. Halfman, *Aeroelasticity*, Addison-Wesley Publishing Company Inc., (1995).

8. Acknowledgement

This work was funded by the EPSRC through grant GR/L95175. The authors are also grateful for the support from BAE Systems and also Glasgow University for providing the CFD Code.

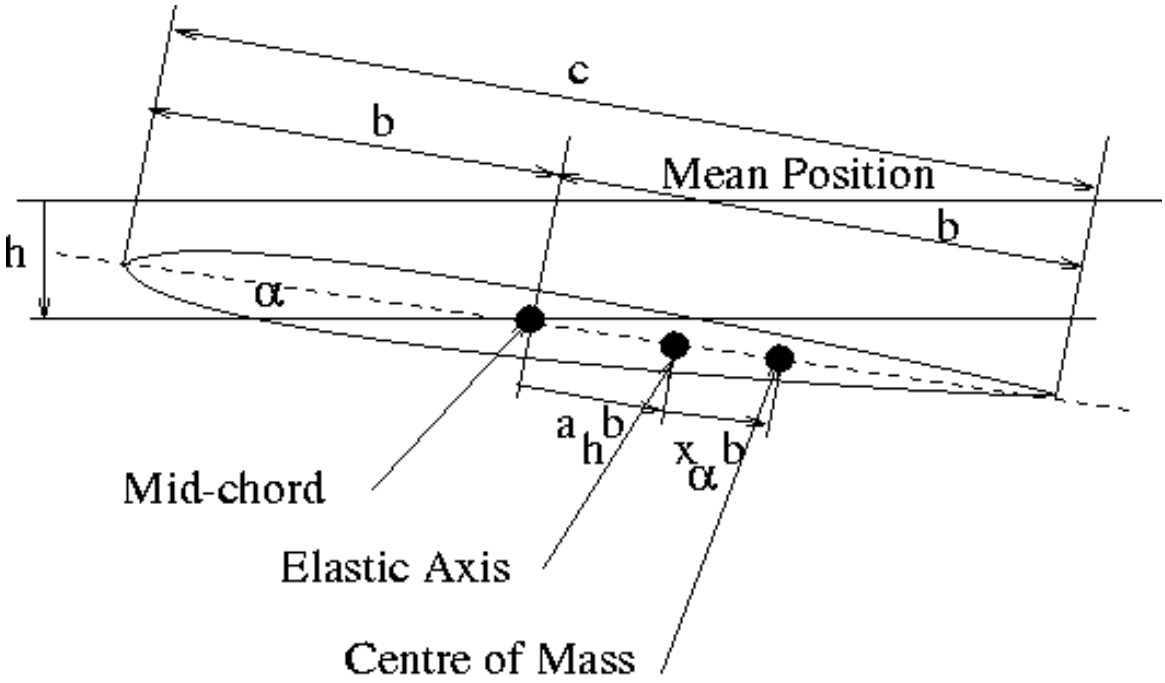

Figure 1. Aerofoil geometry for two degrees of freedom motion.

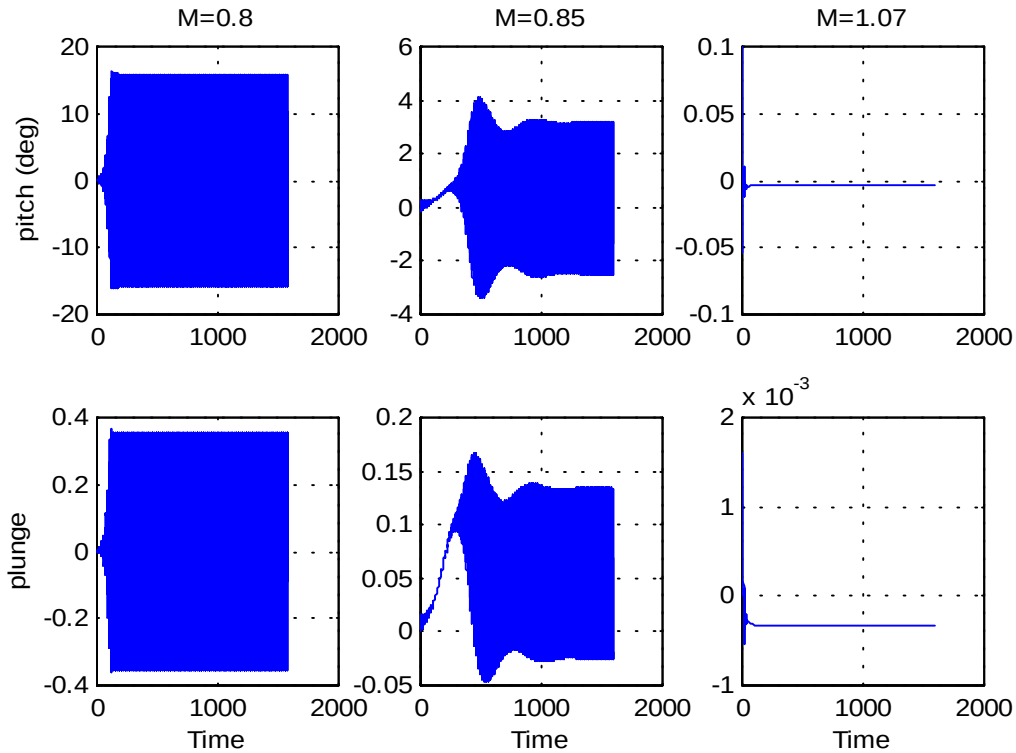

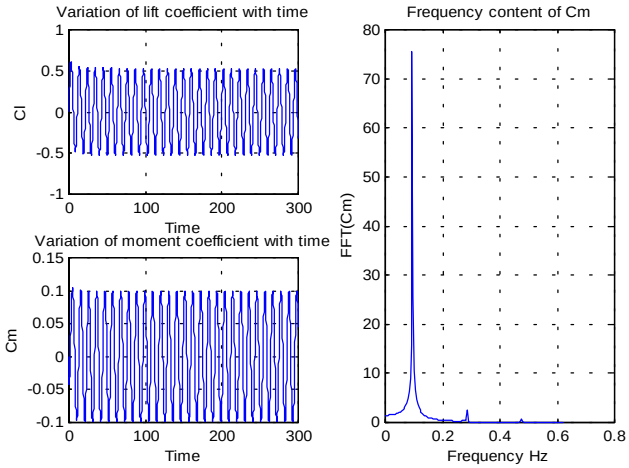

Figure 3. C_l and C_m time histories and frequency content of C_m at M=0.8.

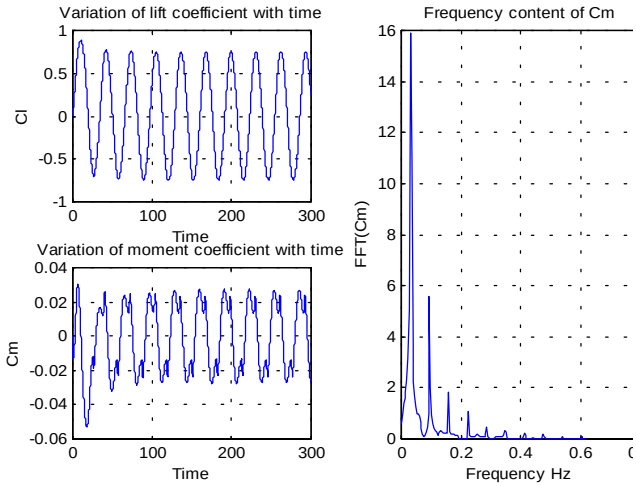

Figure 4. C_l and C_m time histories and frequency content of C_m at M=0.85.

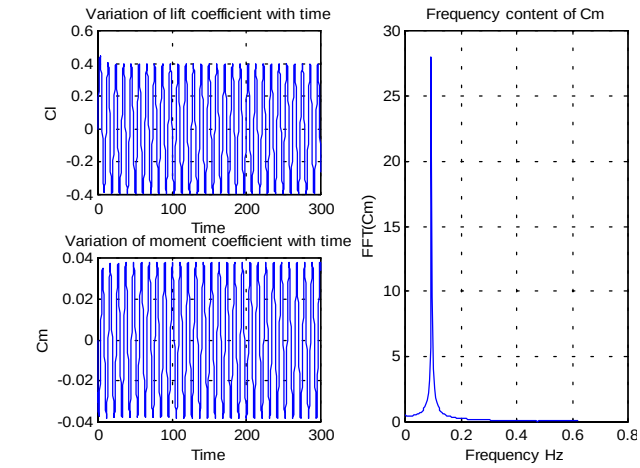

Figure 5. C_l and C_m time histories and frequency content of C_m at M=1.07.

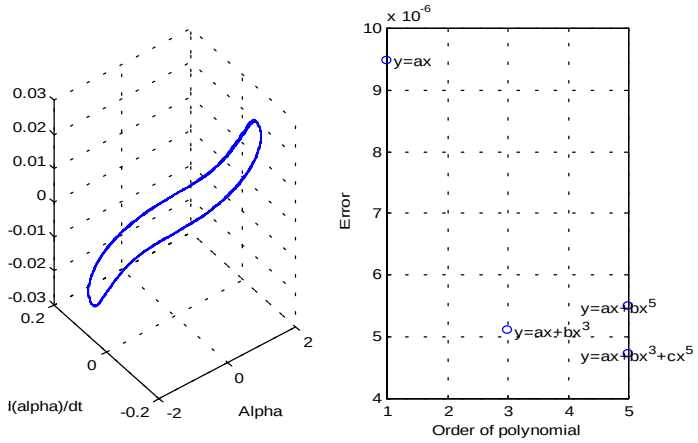

Figure 6. Restoring force plot for C_m using CFD results and the corresponding error plot for different order of polynomials.

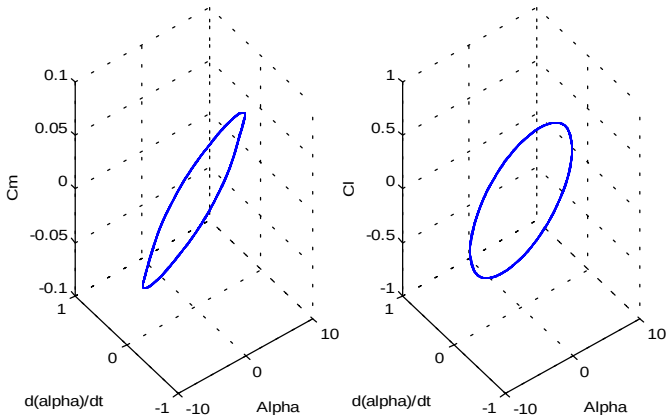

Figure 7. Restoring force plots for C_l and C_m for a forced amplitude of 6° at M=0.8.

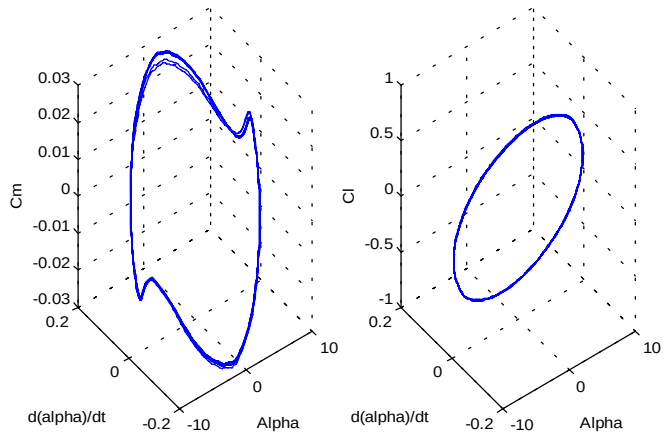

Figure 8. Restoring force plots for C_l and C_m for a forced amplitude of 6° at M=0.85.

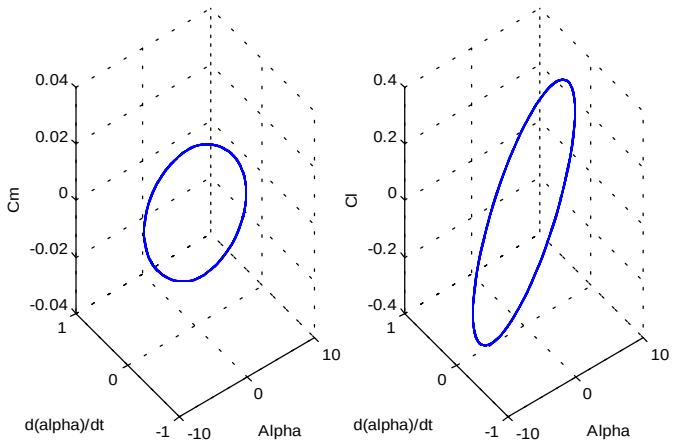

Figure 9. Restoring force plots for C_l and C_m for a forced amplitude of 6° at M=1.07.

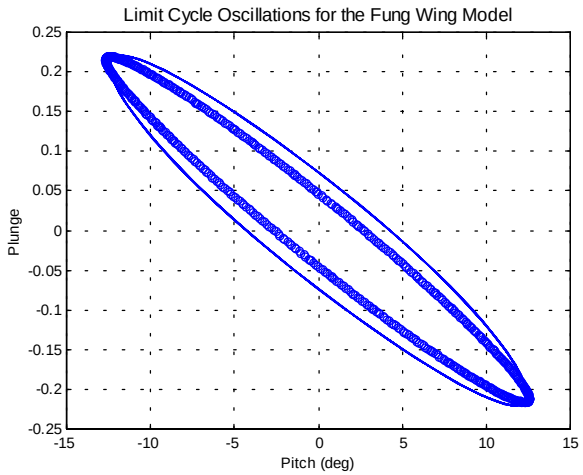

Figure 10. Comparison of LCO's amplitude obtained from CFD (ooo) and aeroelastic model (—).